DIMITRI V4 Algorithm Theoretical Basis Document: Sensor-to-simulation intercomparison over Desert Pseudo-Invariant Calibration Sites (PICS)

Reference: ARG_DIM_QA4EO_TN_Desert_PICS

Version: 1.2

Date: 1st December 2023

	Name	Company/Organization	Signature	Date
Prepared by	Bahjat Alhammoud Marc Bouvet	ARGANS Ltd (UK) ESA/ESTEC		30/10/2023
Reviewed by	Marc Bouvet	ESA/ESTEC		
Approved by	Marc Bouvet	ESA/ESTEC		

Table of Contents

List of Figures

List of Tables

Version History

Version	Date	Main changes
1.0	14/01/2016	First issue of this document by Marc Bouvet
1.1	25/10/2023	Updated version, including: - the small-Desert PICS coordinates - BRDF-impact on the outputs and Correction-LUTs -
1.2	1/12/2023	Updated version, slight editing to section 8

Reference documents

ID	Reference
RD.1	Bouvet M., Radiometric comparison of multispectral imagers over a pseudo-invariant calibration site using a reference radiometric model, Remote Sensing of Environment 140 (2014) 141–154
RD.2	Bouvet M., DIMITRI ATBD: Sensor-to-simulation intercomparison over Pseudo-Invariant Calibration Sites , issue 1.0 (14/01/2016)

Acronyms

ATBD Algorithm Theoretical Basis Document
BRDF bidirectional reflectance distribution function
COT Cloud Optical Thickness
DIMITRI The Database for Imaging Multi-spectral Instruments and Tools for Radiometric Intercomparison
ECMWF European Center for Medium-Range Weather Forecasts
EO Earth Observation
ESA European Space Agency.
GML Geography Markup Language
MSI Multi Spectral Instrument
NIR Near InfraRed
PDF Probability Distribution Function
PICS Pseudo Invariant Calibration Sites
RAA Relative Azimuth Angle
ROI region of interest
RT Radiative Transfer
RTM Radiative Transfer Model
SAA Sun azimuth angle
SWIR ShortWave InfraRed
SZA Solar Zenith Angle
TCO total column ozone
TIR Thermal InfraRed
TOA Top-Of-Atmosphere
VAA viewing azimuth angle
VIS Visible
VNIR Visible and Near InfraRed
VZA Viewing Zenith Angle
WV Water Vapor
XML Extensible Markup Language

Scope of the document

This document describes the Algorithm Theoretical Basis Document (ATBD) for the simulation of the TOA reflectance observation of any sensor ingested in DIMITRI over 6 Pseudo Invariant Calibration Sites (PICS) by the so-called (ARGANS) desert methodology implemented in DIMITRI in the framework of the ESA contract N°: 400011454/15/I-SBo and its CCN1.

1. Introduction

A set of six desert sites (referred to as Algeria 3, Algeria 5, Libya 1, Libya 4, Mauritania 1 and Mauritania 2) called the Pseudo Invariant Calibration Sites (PICS) was selected by the Committee on Earth Observation Satellites (CEOS) among 20 sites originally identified by Cosnefroy et al. (1996) as desert sites suitable for "*multitemporal, multiband, or multiangular calibration of optical satellite sensors"*. All sites are located in the Sahara and were chosen chiefly for their potential radiometric stability.

The absence or scarcity of vegetation on these sites generally leads to the assumption that their surface Bidirectional Reflectance Distribution Function (BRDF) should be temporally stable but the atmosphere remains variable in terms of absorbing gases concentrations, aerosol optical properties and physical properties (e.g.: temperature, pressure).

Although the surface BRDF is assumed radiometrically stable in time, it is not expected to be Lambertian. At top-of-atmosphere (TOA) reflectance level, the combination of BRDF angular variability and atmospheric temporal/angular variability leads to satellite TOA reflectance varying from acquisition to acquisition. Such atmospheric temporal variability and surface/atmospheric geometrical variations can impact the TOA signal in a significant fashion. They should be corrected for by modelling the TOA signal in order to fully exploit the PICS assumed radiometric stability for the radiometric monitoring of EO multispectral sensors.

The document is split into several sections:

- Section 2 provides an overview of the approach proposed to simulate TOA reflectance over the PICS
- Section 3describes the selection of the MERIS data for the retrieval of the PICS surface BRDF
- Section 4 describes the inversion of both the aerosol optical properties (and load) and the surface BRDF over the PICS
- Section 5 describes the generation of hyperspectral BRDFs for each PICS from the BRDFs derived in MERIS spectral bands
- Section 6 explains how the hyperspectral BRDFs obtained at each site are used to simulate hyperspectral TOA reflectances at each site and ultimately TOA reflectance from any sensor

- Section 7 describes how the hyperspectral reflectance model is run to simulate MERIS full archive observations of the PICS 9
- Section 8 describes the simulation of MERIS TOA observations over the small-PICS
- Section 9 discusses known limitations of the TOA simulations
- Section 10 discusses uncertainties
- Section 11 is devoted to the conclusion

2. Overview of the approach to simulated Toa reflectance over the PICS

A model is proposed to simulate the TOA reflectance in the visible to near-infrared (NIR) spectral range over the 6 PICS identified by CEOS. This model is described in Bouvet (2014). It extends through the MERIS spectral range (about 400 nm to 900 nm). It is based on a fully physical radiative transfer model simulating the coupling between a realistic atmosphere and a spectral surface Bidirectional Reflectance Distribution Function (BRDF) model parameterized by 4 free parameters. The model is 'calibrated' over each PICS site using 4 years of MERIS observations between 2006 and 2009 included. This 'calibration' process actually consists of retrieving for each site the surface BRDF model in each MERIS spectral band. This surface BRDF model retrieval is also described in Bouvet (2014). In the latter paper, the retrieval of the surface BRDF was done assuming a constant set of aerosol optical properties (so-called 'average continental') and a constant aerosol optical thickness at 550 nm (0.2). In the present document, an evolution of this 'calibration' process is described: rather than retrieving the BRDF in each MERIS spectral band independently by assuming fixed aerosol properties, the aerosol optical properties are now retrieved in the MERIS bluest bands (412 nm) and then further used for the BRDF retrieval in all MERIS spectral bands.

3. Selection of MERIS data used to retrieve the surface BRDF model parameters over the PICS

MERIS L1 data from the 3rd reprocessing covering a 4-year period from 01/01/2006 to 31/12/2009 were extracted from the freely available Database for Imaging Multi-spectral Instruments and Tools for Radiometric Intercomparison (DIMITRI) (http://www.argans.co.uk/dimitri/). These data consist of TOA reflectances averaged over the regions of interest (ROI) in Table 1. Following Bouvet (2014), the L1 data were corrected for the instrument smile effect (irradiance correction only following Bourg et al. (2008)). They were automatically cloud screened following the MERIS-GlobCarbon scheme as per Plummer (2008). Conversely to Bouvet (2014), the data were not further visually screened. About 400 MERIS acquisitions are available after this data screening for each PICS. Clouds are more frequent over the site during the winter months resulting into more acquisitions being available at low sun zenith angles (SZAs) than for high SZAs. To avoid over-constraining the inversion of the surface BRDF model at low SZAs at the expense of high SZAs, a sub-selection of 200 of these

cloud free MERIS TOA observations is done at times randomly selected and uniformly spread across the 4-year period.

For each acquisition, the following data are automatically extracted from the DIMITRI database: the mean TOA reflectance over ROI, the standard deviation of the TOA reflectance within the ROI, the sun and viewing direction zenith and azimuth angles (SZA, VZA, SAA, VAA), the total columnar ozone (TCO) and the total column water vapour (WV)). These TCO and WV available in the DIMITRI database correspond to the meteorological data available in the MERIS L1 products. They are data from the European Center for Medium-Range Weather Forecasts (ECMWF) operational Numerical Prediction Weather (NWP) model. They were substituted by the corresponding ECMWF ERA-Interim reanalysis data (see description in Dee et al. (2011)).

Site name	North Latitute	South Latitude	East Longitude	West Longitude
Algeria-3	30.82	29.82	8.16	7.16
Algeria-5	31.52	30.52	2.73	1.73
Libya-1	24.92	23.92	13.85	12.85
Libya-4	29.05	28.05	23.89	22.89
Mauritania-1	19.9	18.9	-8.8	-9.8
Mauritania-2	21.35	20.35	-8.28	-9.28

Table 1: The definition of the regions of interest over the 6 PICS.

4. Inversion of the surface BRDF model parameters at each MERIS spectral bands over the PICS

In this section we describe the evolution of the surface BRDF retrieval scheme described by Bouvet (2014). For reminder, the retrieval of the surface BRDF simply is an optimisation process of the cost function described below.

4.1. Retrieval of aerosol optical properties and thickness at 412 nm

Why choosing the MERIS 412 nm band to retrieve aerosol optical properties and thickness? Bouvet (2014) (section 3.5.1.5) briefly discusses the impact of the aerosol optical properties and aerosol optical thickness on the simulated TOA reflectance in MERIS spectral bands. The bluest bands appears to be the most sensitive to changes in aerosol optical properties: if the same AOT value at 550 nm of 0.2 used for the inversion of the BRDF parameters over the Libya-4 site is re-used to simulate the MERIS TOA observations but the assumed 'average continental' aerosol model is substituted by the so-called 'desert' aerosol model (see Hess (1998)) to re-simulate the 200 MERIS

observations, a decrease of nearly 6 % of the TOA signal in the blue and an increase of 2 % towards the red and NIR are obtained.

To retrieve the aerosol optical properties and thickness from the MERIS TOA reflectance at 412 nm, the retrieval of the BRDF model parameters is carried out exactly as described in Bouvet (2014) but successively for two aerosol optical models (the 'average continental' and 'desert' aerosol models from Hess (1998)) and 5 aerosol optical thickness at 550 nm (0.0, 0.1, 0.2, 0.3 and 0.5). This results in 2 x 5 = 10 values of the RMSE in % (412 nm) between the MERIS simulated and measured TOA reflectances being obtained by the surface BRDF model parameter inversion scheme (and as well 10 correspoding sets of surface BRDF model parameters). The combination of aerosol model and optical thickness resulting in the lowest RMSE is selected as being representative for the PICS. Only this combination is then used for the retrieval of the surface BRDF model parameters in the other MERIS spectral bands.

Figure 1 shows the 10 values for the RMSE values obtained for each site in MERIS 412 nm band. The error bars are associated to the standard deviation obtained for multiple retrieval of the surface BRDF model parameters initiated with differing initial values of the RPV parameter ρ_0 (see Bouvet (2014)). For a discussion on the initialisation of Table 2 gives the aerosol model and aerosol optical thickness at 550 nm retrieved at each site.

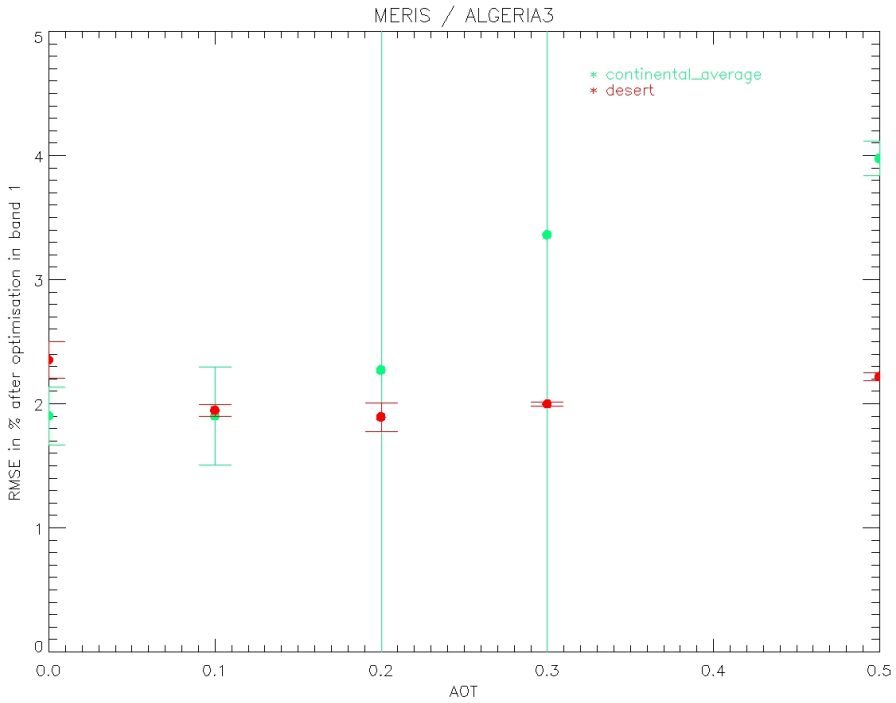

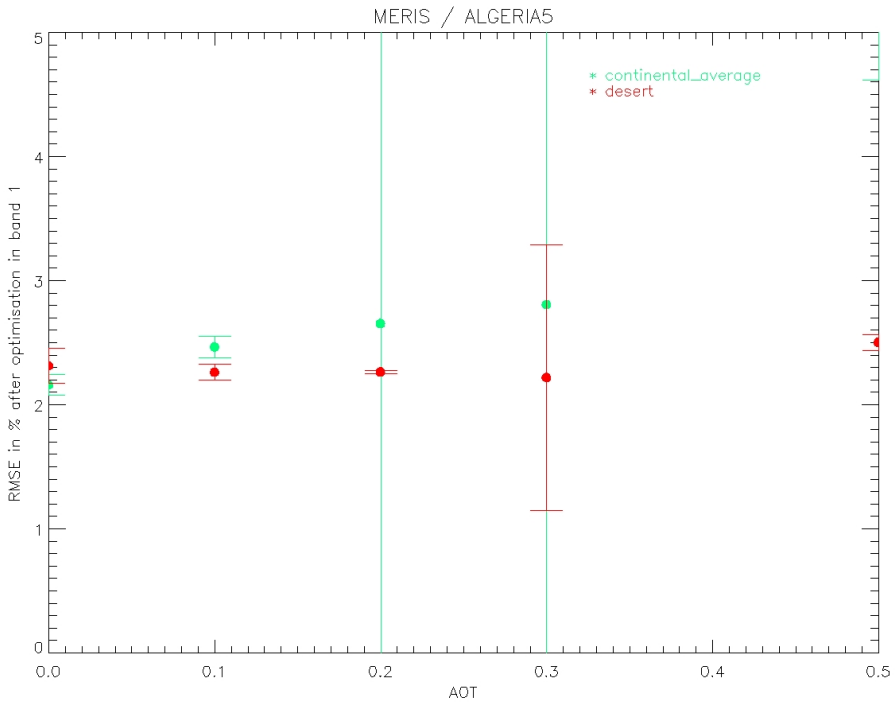

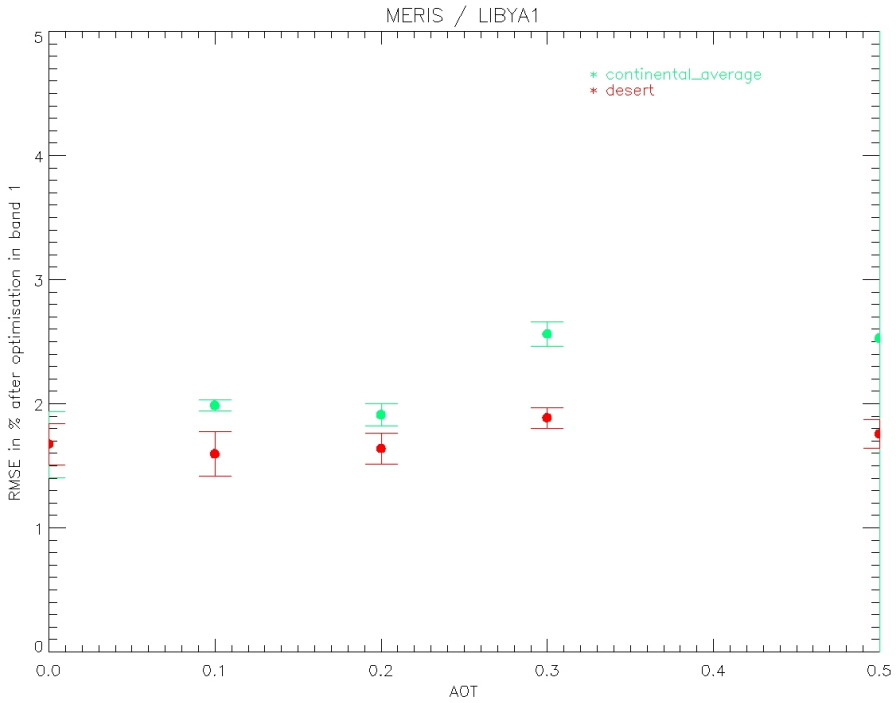

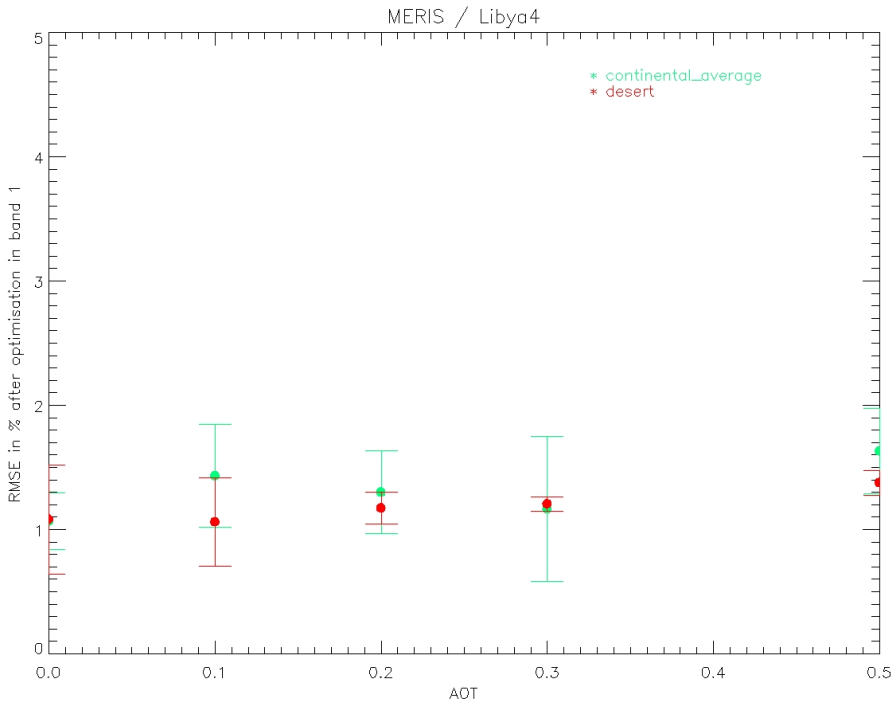

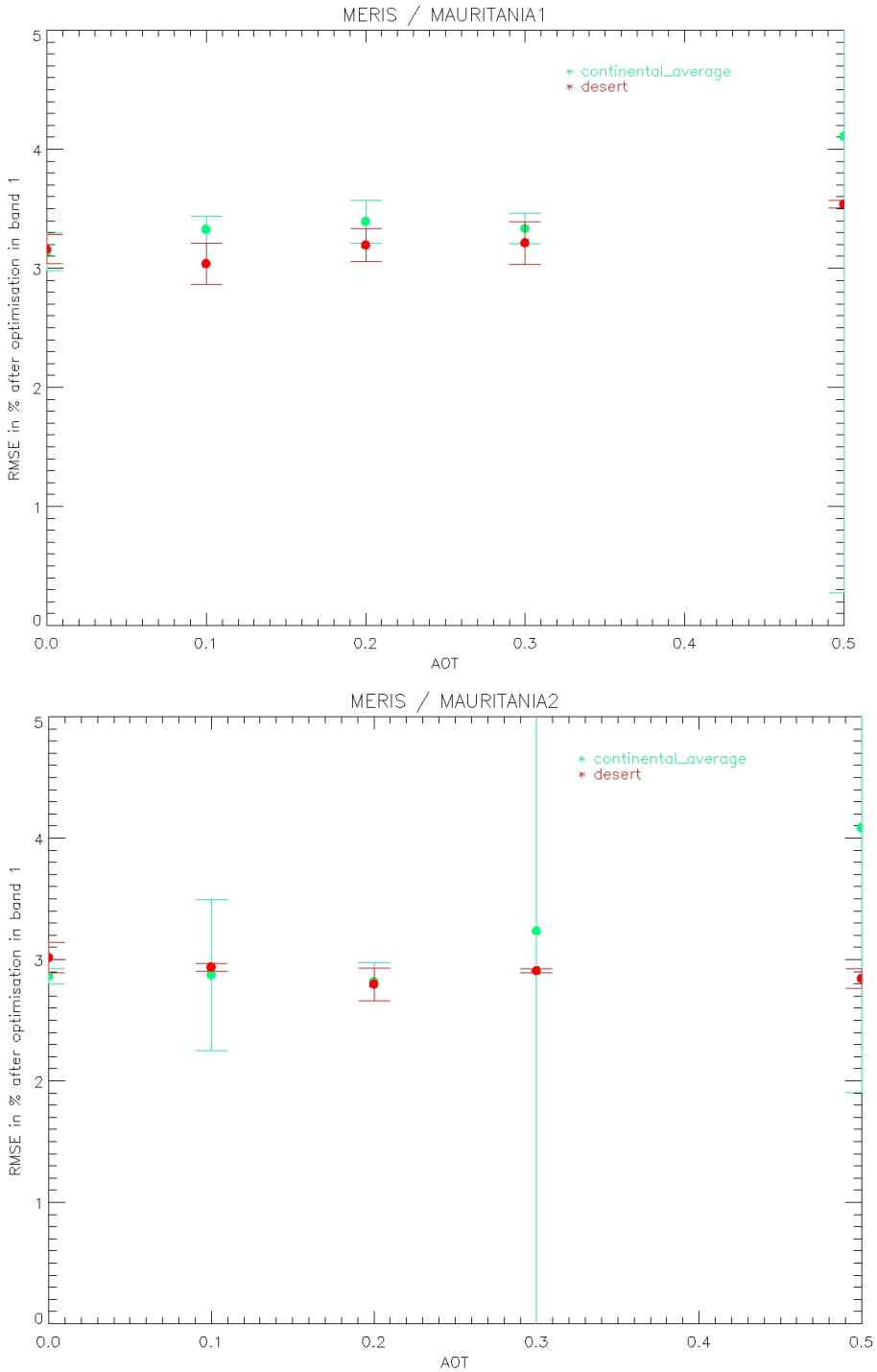

Figure 1. The aerosol model and aerosol optical thickness inversion results for each site. The figures show the RMSE (between the $\rho_{sim}^{TOA}(412\ nm)$and $\rho_{obs}^{TOA}(412\ nm)$ for 200 selected MERIS observations) obtained at the end of the inversion of the surface BRDF model parameters at 412 nm for various AOT at 550 nm and the two aerosol model 'continental average' and 'desert'. The error bars are associated to the standard deviation obtained for multiple retrieval of the surface BRDF model parameters initiated with differing initial values of the RPV parameter ρ_0.

Site name	Aerosol model	AOT at 550 nm
Algeria-3	Desert	0.2
Algeria-5	Continental-average	0.0
Libya-1	Desert	0.1
Libya-4	Desert	0.1
Mauritania-1	Desert	0.1
Mauritania-2	Desert	0.2

Table 2: The aerosol model and aerosol optical thickness at 550 nm retrieved at each PICS.

4.2. Results of the inversion of the surface BRDF model parameters at the PICS

The RPV model proposed by Rahman et al. (1993) is a parametric BRDF model representing BRDFs. It is represented by the product an amplitude ρ_0 of three separate functions accounting for both the illumination and viewing directions:

$$\rho(\theta_0,\theta_V,\Delta\phi,\rho_0,k,\Theta,\rho_c) = \rho_0\, M_1(\theta_0,\theta_V,k)\, F_{HG}(\mathrm{g},\Theta) H(\rho_c,G) \quad (1)$$

Where

$$M_1(\theta_0,\theta_V,k) = \frac{cos^{k-1}\theta_0 cos^{k-1}\theta}{(cos\theta_0+cos\theta)^{1-k}} \quad (2)$$

$$F_{HG}(\mathrm{g},\Theta) = \frac{1-\Theta^2}{(1+2\Theta cosg+\Theta^2)^{3/2}} \quad (3)$$

$$H(\rho_c,G) = 1+\frac{1-\rho_c}{1+G} \quad (4)$$

$$cosg = cos\theta_0 cos\theta + sin\theta_0 sin\theta cos\Delta\phi \quad (5)$$

$$G = (tan^2\theta_0 + tan^2\theta - 2tan\theta tan\theta_0 cos\Delta\phi)^{1/2} \quad (6)$$

where θ and θ_0 are the VZA and SZA, respectively. In the above formulation the relative azimuth angle $\Delta\phi$ is zero when the source of illumination is behind the sensor. The model is parameterized by 4 parameters: ρ_0, k, Θ and ρ_c.

The results for ρ_0, k, Θ and ρ_c at each PICS can be seen in Figure 2. On top of the at-MERIS-spectral band values of the BRDF model parameters, the retrieved hyperspectral variations are also shown in red. The derivation of the hyperspectral variations of the parameters in described in the section 5.

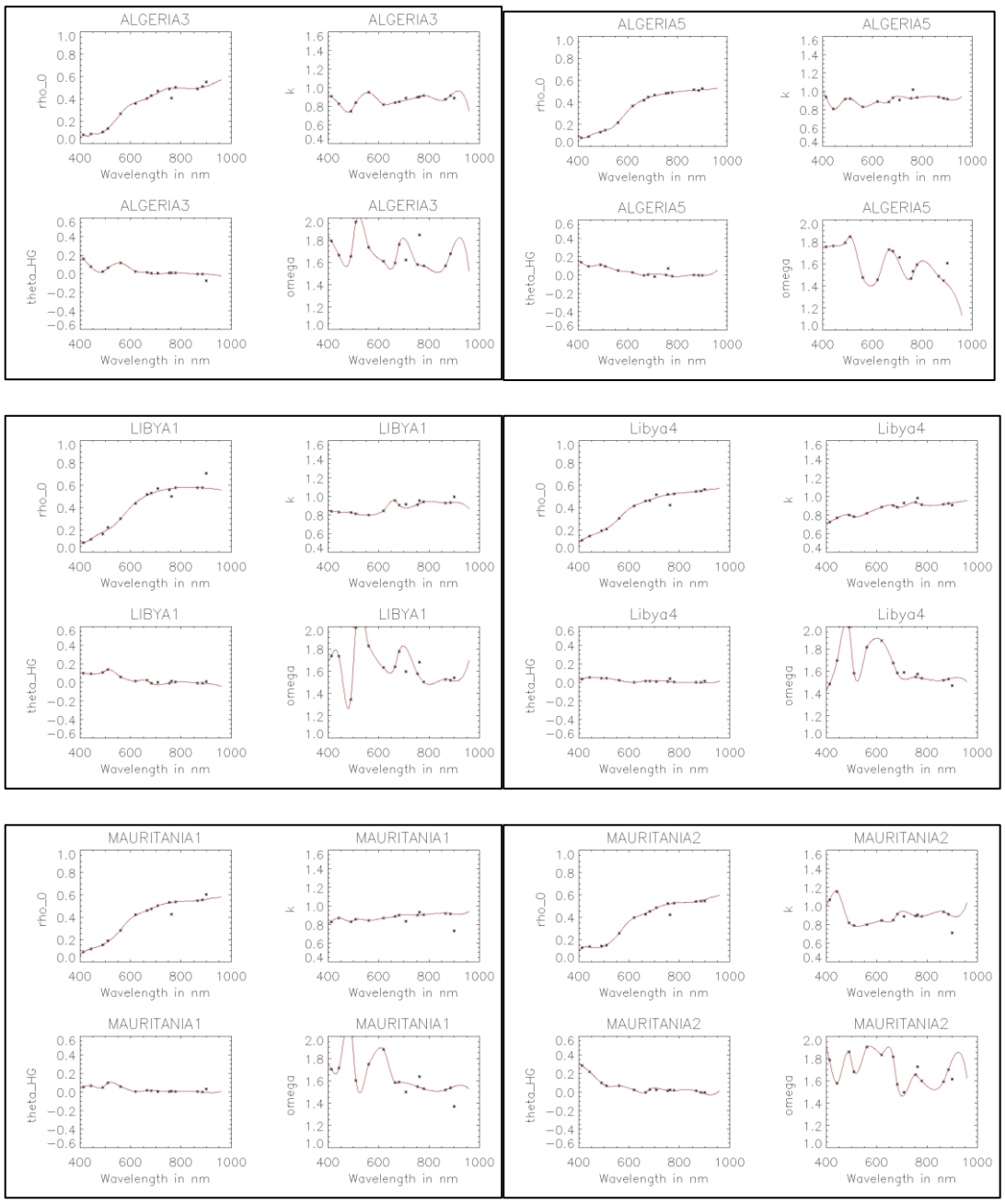

Figure 2. The spectral variations of the RPV BRDF model parameters at each MERIS spectral band inverted from the MERIS TOA reflectance observations (black stars). In red, their spectral interpolation (in red). For each site, from left to right and from top to bottom, ρ_0, k, Θ and the ratio $\omega = {}^{\rho_c}/_{\rho_0}$

The retrieval of the surface BRDF simply is an optimisation process of the cost function:

$$RMSE\ in\ \%(\lambda) = \chi = \sum_{i=1}^{200} \sqrt{{}^{1}/_{200}\left[\frac{\left(\rho_{sim}^{TOA}(i,\lambda) - \rho_{obs}^{TOA}(i,\lambda)\right)}{\rho_{obs}^{TOA}(i,\lambda)} \times 100\right]^2} \qquad (7)$$

Where $\rho_{sim}^{TOA}(i,\lambda)$ and $\rho_{obs}^{TOA}(i,\lambda)$ are the simulated and observed TOA reflectance respectively and *i* is the observation index ranging from 1 to 200 and λ is the spectral band ranging from 1 to 15.

The $\rho_{sim}^{TOA}(i,\lambda)$ are derived from simulations based on the MYSTIC radiative transfer model (for details on the model, see section 3.1 of Bouvet (2014)).

The RMSE between the $\rho_{sim}^{TOA}(i,\lambda)$ and $\rho_{obs}^{TOA}(i,\lambda)$ obtained at the end of the surface BRDF model parameter inversion are shown in Figure 3.

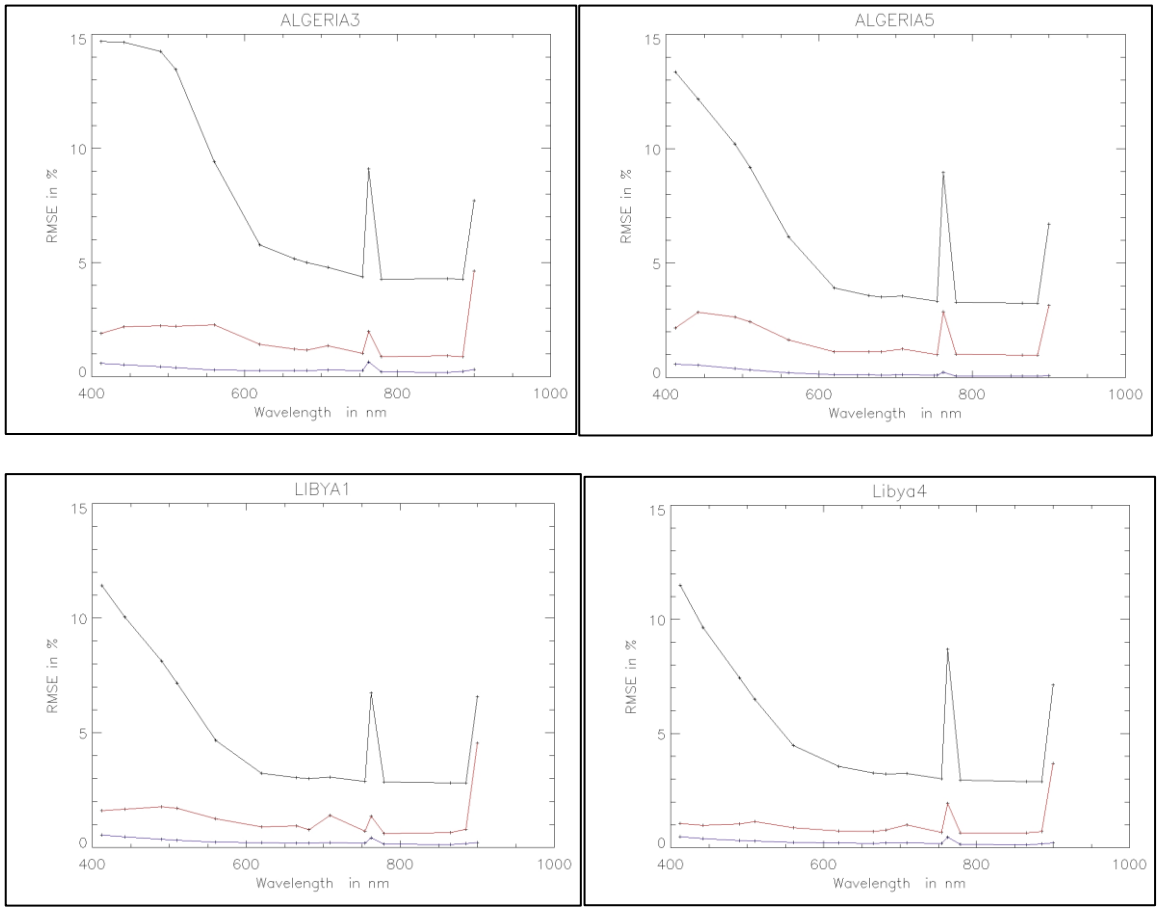

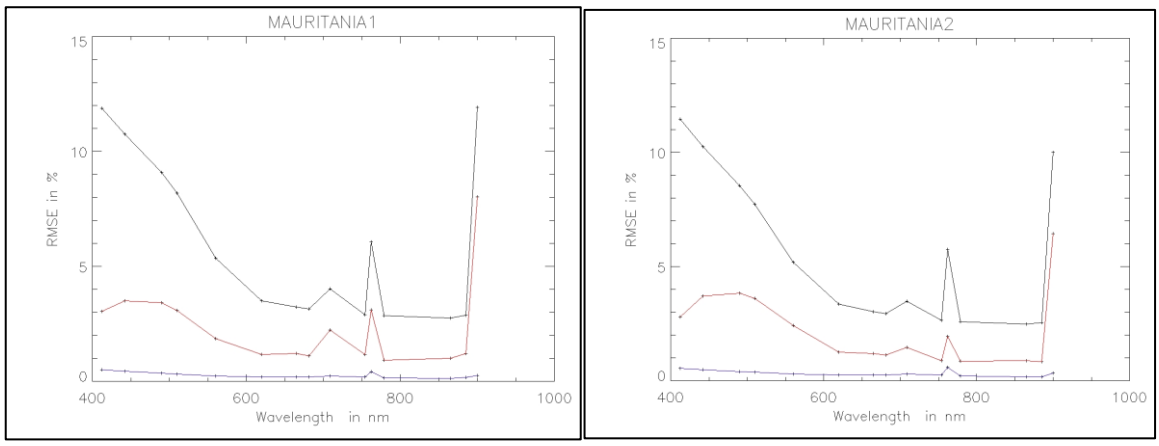

Figure 3. The spectral variations of the RMSE between the MERIS TOA reflectance simulations and the observations is shown in red. In black, the MERIS TOA reflectance standard deviation for the 4 year period. In blue, the mean photon noise associated to a single simulation of a MERIS TOA reflectance observation.

The mean bias between the $\rho_{sim}^{TOA}(i,\lambda)$ and $\rho_{obs}^{TOA}(i,\lambda)$ obtained at the end of the surface BRDF model parameter inversion are shown in Figure 4.

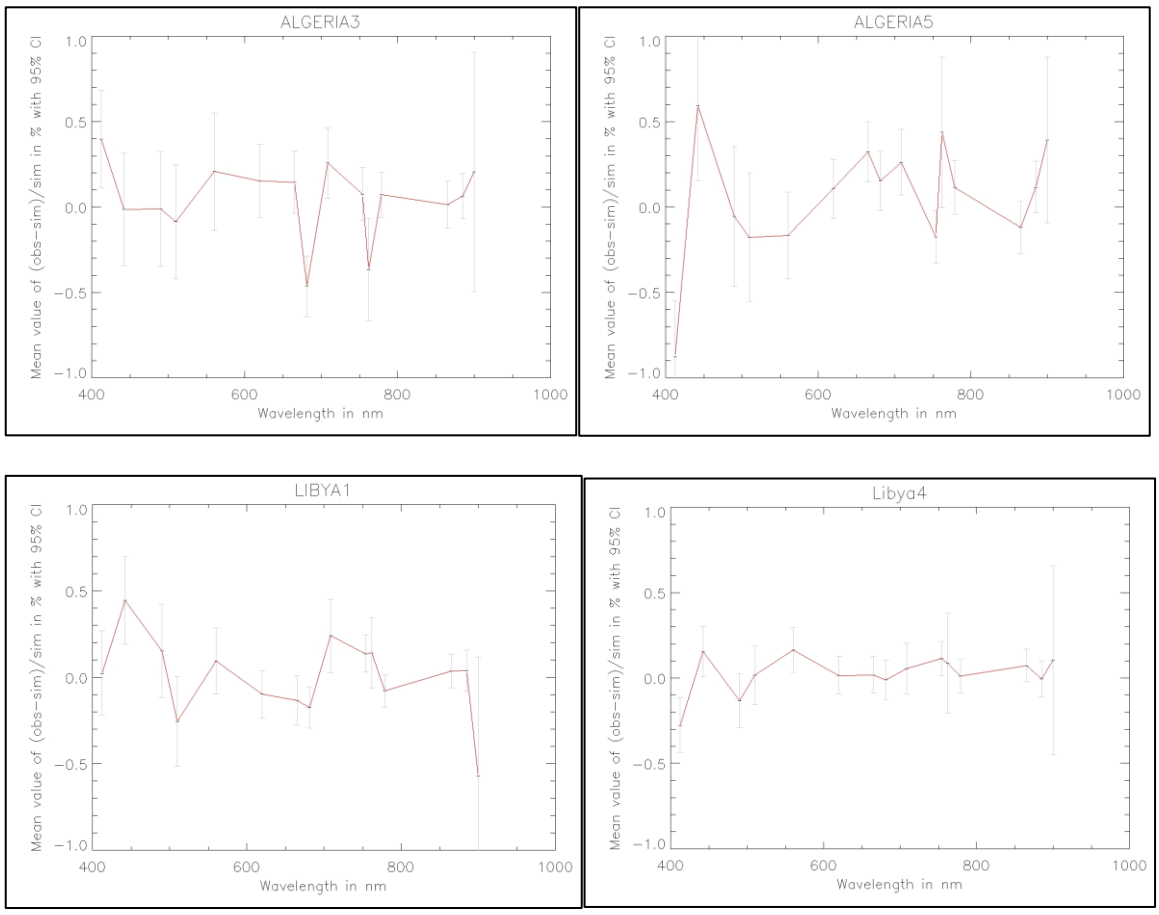

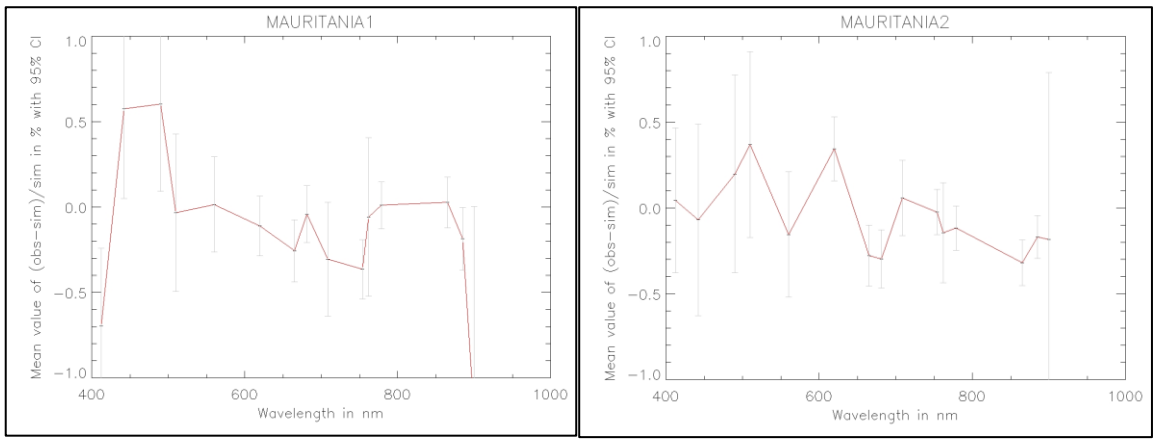

Figure 4. The mean relative difference between the MERIS observation and their simulation and the associated uncertainty of the mean (95 % CI, see Bouvet (2014)).

5. Generation of hyperspectral surface BRDF from MERIS surface BRDF model

Figure 5 is used to fit the MERIS the ρ_0 parameter spectral variations. The spectral variations of the 3 other BRDF model parameters (k, Θ and the ratio $\omega = {\rho_c}/{\rho_0}$) are obtained by simple spline interpolation. The interpolation of the BRDF model parameters is done excluding spectral band for which the water vapour and O2 absorption is significant (band 9, 11 and 15).

The results are shown in Figure 2 individually for each site and for all sites together in

Figure 6.

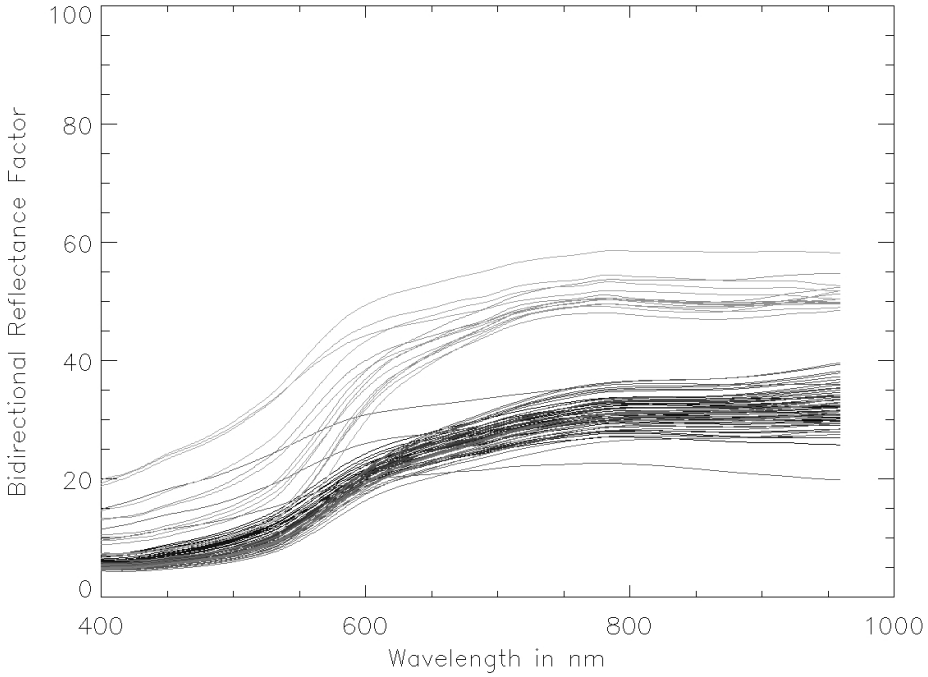

Figure 5: All BRF sand spectra measured on samples collected at the Simpson desert (Australia), Muleshoe (Texas, USA) and in the Namibian desert. Illumination is at 45 degrees and measurement at nadir from Bullard et al. (2002)) and White et al. (2009)

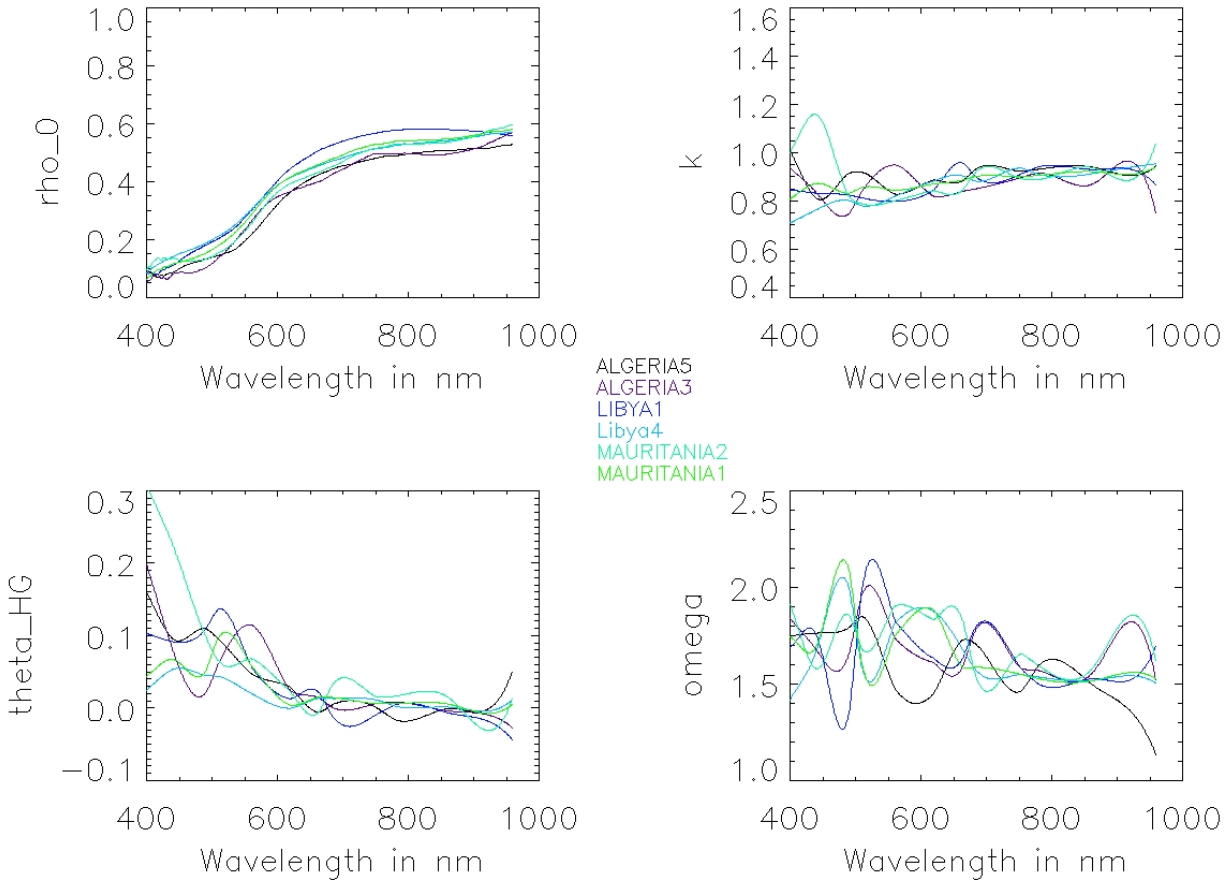

Figure 6: The spectral variations of the hyperspectral RPV BRDF model parameters. From left to right and from top to bottom, ρ_0, k, Θ and the ratio $\omega = {}^{\rho_c}/_{\rho_0}$.

6. Simulation of TOA observations over the PICS for any sensor

The previous described hyperspectral surface BRDF models and aerosol optical properties retrieved over each site can be used as input to simulate the hyperspectral TOA reflectance over the site which in turn, after convolution with the sensor spectral response can be used to simulate the in-band TOA reflectance of any sensor observing the sites, in any given geometry.

The L1 data from any sensor to be simulated needs first to be ingested in the DIMITRI database. Only L1 data that are identified as cloud free in the ROI and quality checked are then compared to their simulations. Together with TOA reflectance, the illumination and observation geometry are extracted and used as input to the simulations.

The meteorological data (WV and O3) accompanying the sensor L1 data and extracted in DIMITRI are substituted by the corresponding ERA-Interim data.

7. Verification of the hyperspectral TOA simulations: Simulation of MERIS TOA observations over the PICS

It is interesting to simulate the full archive of MERIS TOA observations over the PICS using the hyperspectral BRDF model parameters derived from 4 years of MERIS data only. This allows assessing the hyperspectral TOA reflectance model ability to reproduce the MERIS observations. Figure 7 shows the time series of the ratio $\frac{\rho_{obs}^{TOA}(\lambda)}{\rho_{sim}^{TOA}(\lambda)}$ over the 6 CEOS PICS sites for the full archive of MERIS 3rd reprocessing data. The mean values of the ratio and associated standard deviations obtained over all 6 PICS sites are provided in Figure 8 in a spectral synthesis.

These results are further discussed in the following sections.

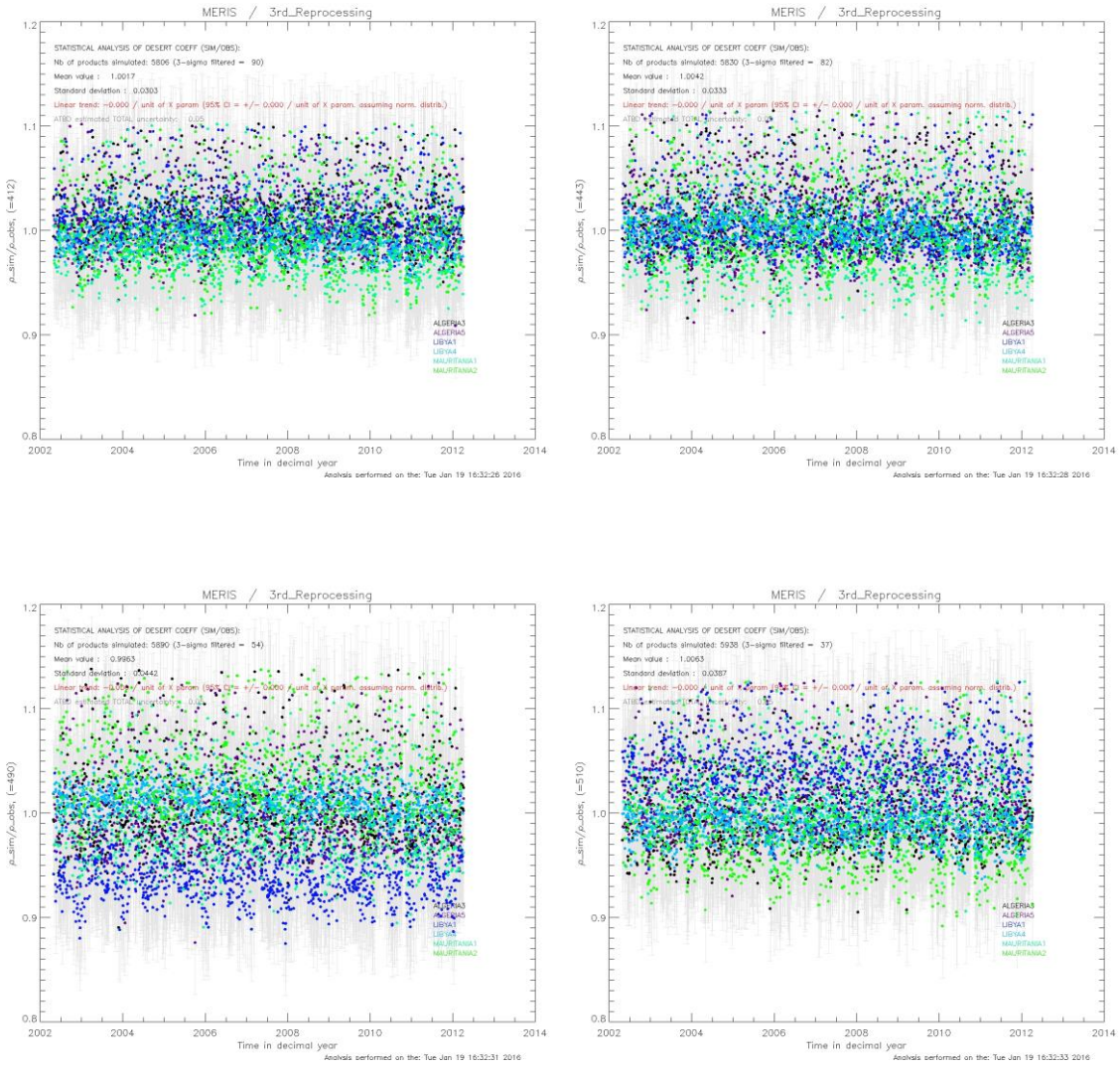

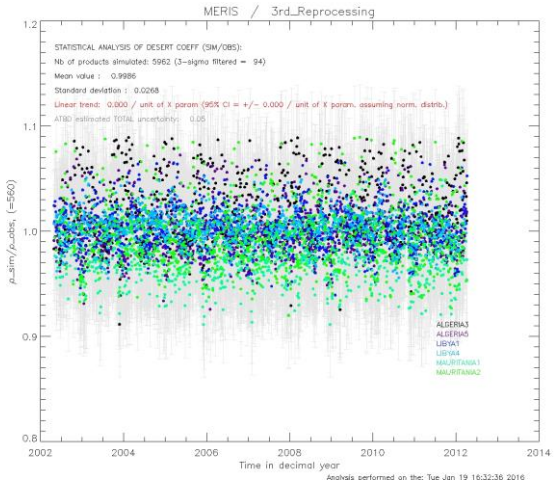

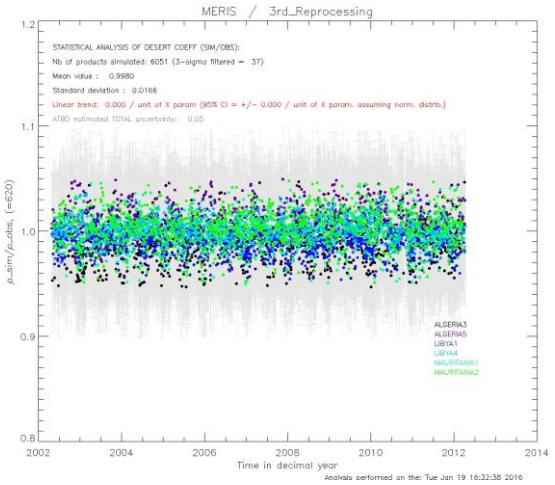

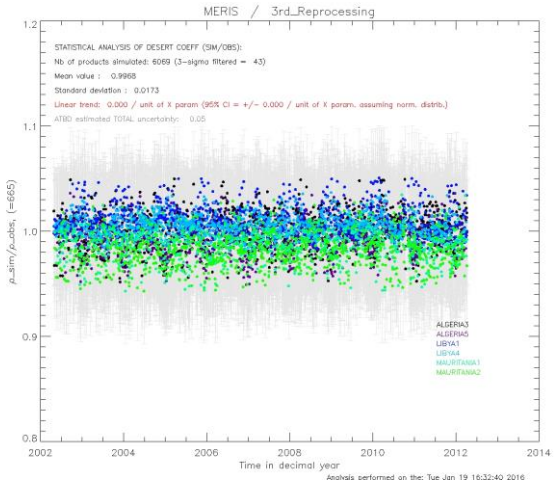

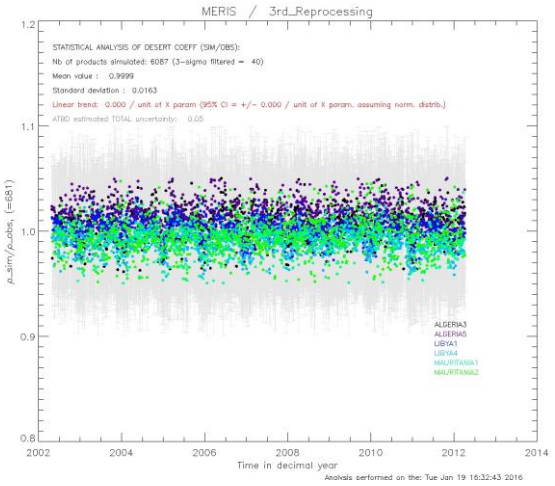

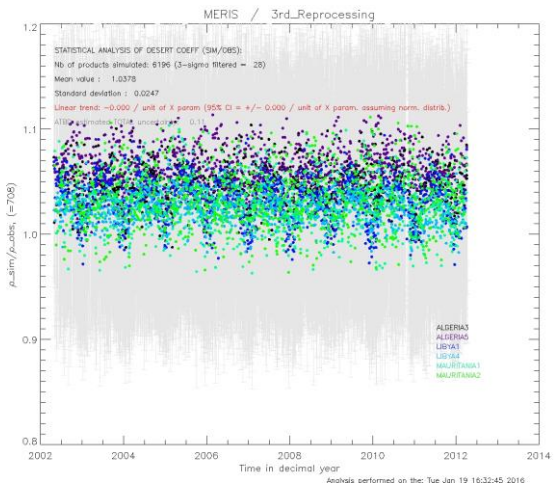

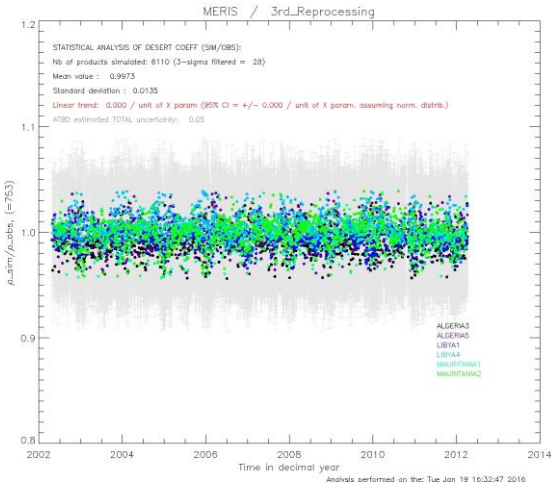

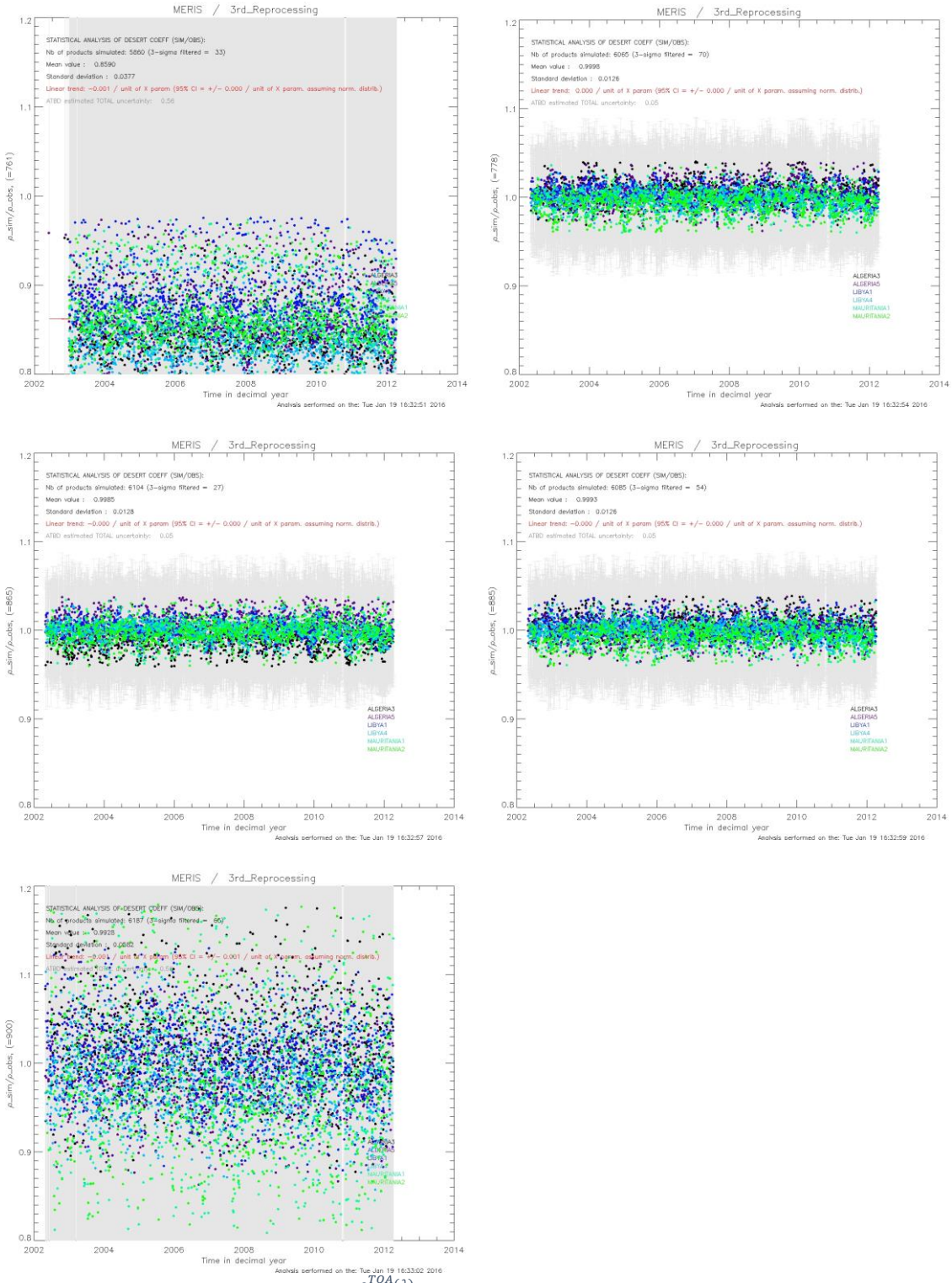

Figure 7: The temporal variations of the ratio $\frac{\rho_{obs}^{TOA}(\lambda)}{\rho_{sim}^{TOA}(\lambda)}$ for MERIS 3rd reprocessing full archive over the 6 PICS sites identified by CEOS. The colour dots correspond to ratios over each site. The grey error bars are the estimated uncertainties.

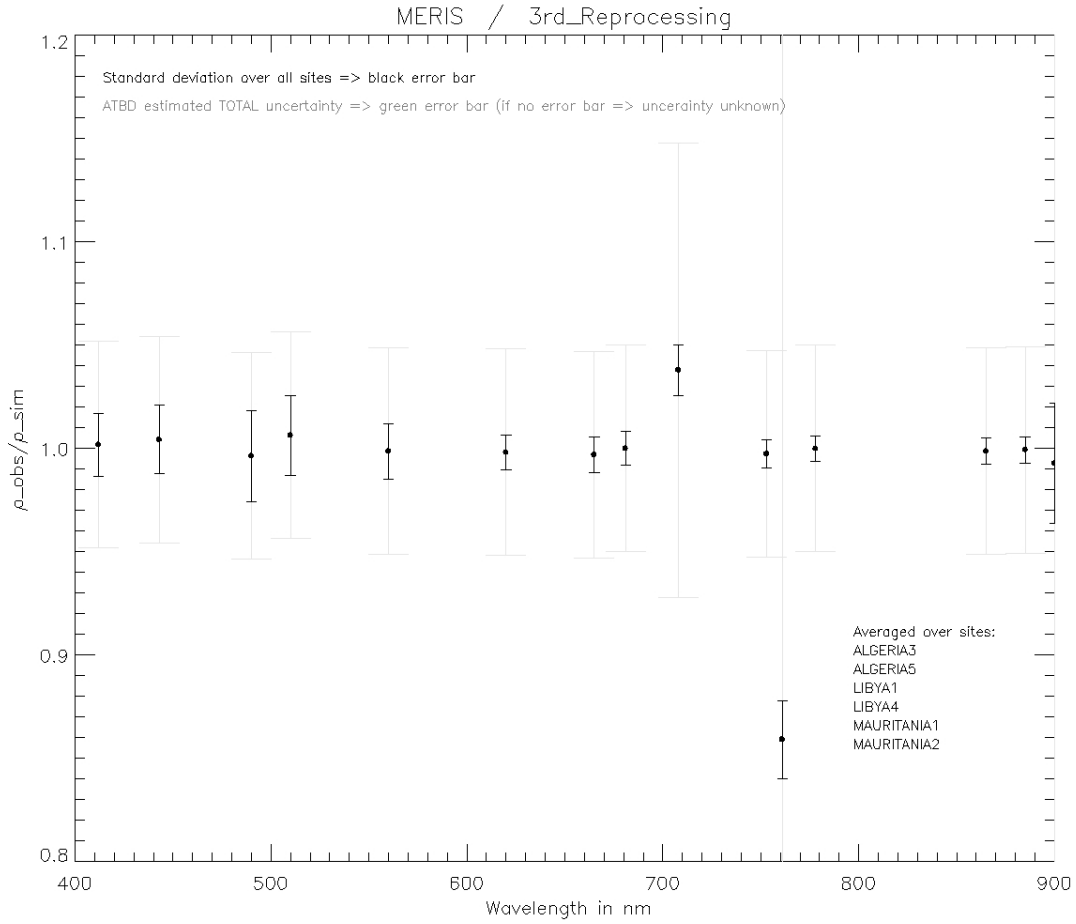

Figure 8: The mean values of the ratio $\frac{\rho_{obs}^{TOA}(\lambda)}{\rho_{sim}^{TOA}(\lambda)}$ for MERIS 3rd reprocessing full archive averaged over the 6 PICS sites identified by CEOS (black dots). The grey error bars are the estimated uncertainties. The black error bar is the standard deviation associated to the mean ratio $\frac{\rho_{obs}^{TOA}(\lambda)}{\rho_{sim}^{TOA}(\lambda)}$ computation.

8. Simulation of MERIS TOA observations over the small-PICS

In order to assess the performance of high-resolution sensors (e.g. Sentinel-2/MSI), smaller regions of 20 x 20 km^2 over PICS are recommended by CEOS-WGCV-IVOS. Hence, it is essential to assess the impact of the BRDF model over the whole archive of MERIS over the small region of interest. Table 3 presents the coordinates of the chosen small PICS included in the recommended 6 desert CEOS-PICS (Table 1). Figure 9 shows the absolute differences of the mean bias, standard deviation, and the trend of the time-series over the 6 CEOS PICS small and large sites for the full archive of MERIS 3rd reprocessing data. The shift values of the mean bias of small to large PICS obtained over the 6 PICS sites are provided in Table 4 in a spectral synthesis.

Site name	North Latitude	South Latitude	East Longitude	West Longitude
Algeria-3_Small	30.50	30.20	7.60	7.30
Algeria-5_Small	31.20	30.90	2.50	2.20
Libya-1_Small	24.80	24.50	13.60	13.30
Libya-4_Small	28.65	28.45	23.49	23.29
Mauritania-1_Small	19.60	19.40	-9.20	-9.40
Mauritania-2_Small	21.05	20.85	-8.60	-8.80

Table 3: The definition of the small regions of interest over the 6 PICS.

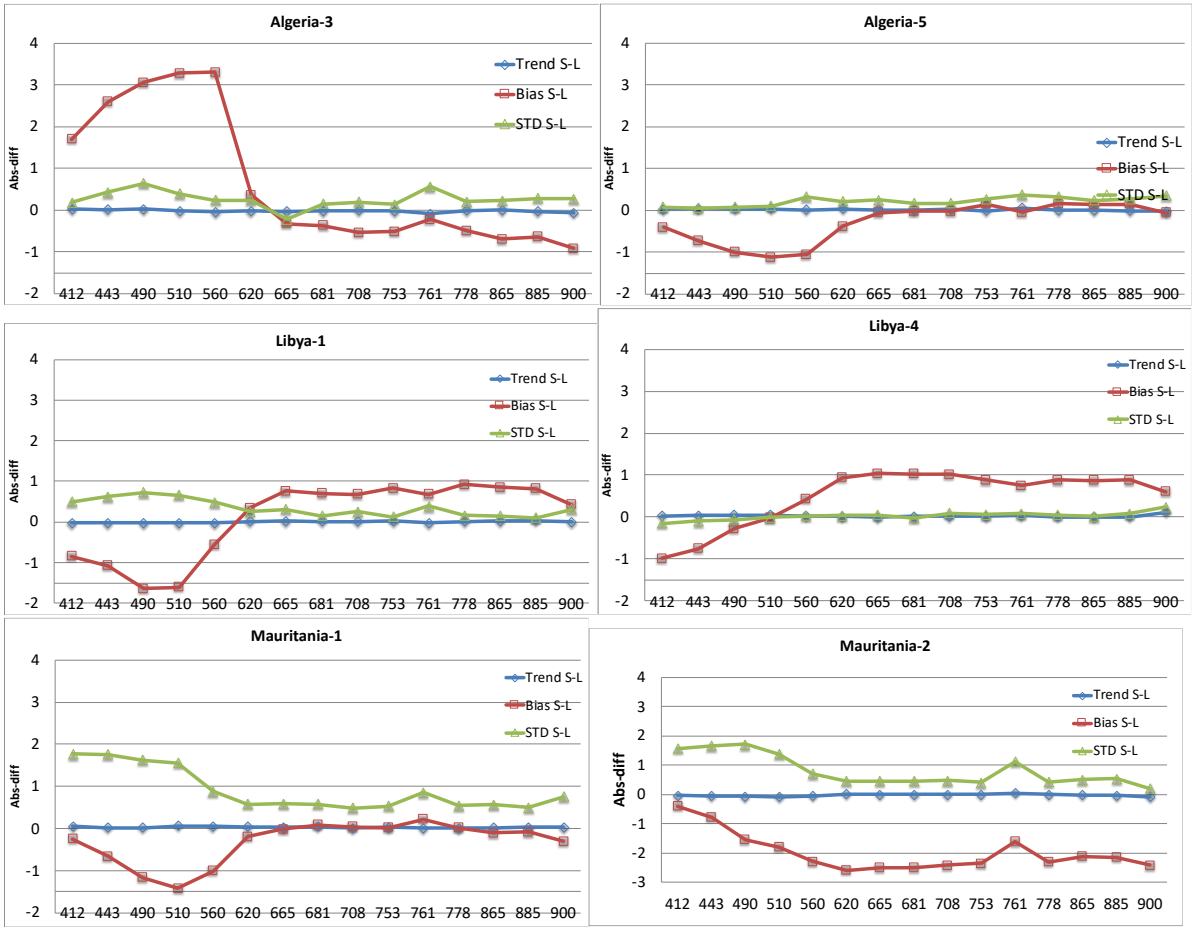

Figure 9: The absolute difference between the small ROIs to the Large ROIs for (red) Bias, (green) Standard deviation and (blue) the trend over the 6 PICS over the whole archive of MERIS 3RP as function of the wavelength.

Site name/ WL (nm)	Algeria3	Algeria5	Libya1	Libya4	Mauritania1	Mauritania2
412	1.69	-0.41	-0.85	-0.99	-0.25	-0.40
443	2.59	-0.73	-1.08	-0.76	-0.66	-0.78
490	3.05	-1.00	-1.64	-0.28	-1.16	-1.54
510	3.28	-1.12	-1.61	-0.02	-1.42	-1.79
560	3.30	-1.06	-0.56	0.42	-1.01	-2.29
620	0.36	-0.38	0.35	0.94	-0.19	-2.59
665	-0.33	-0.06	0.76	1.04	-0.02	-2.50
681	-0.37	-0.02	0.70	1.03	0.09	-2.50
708	-0.54	-0.02	0.68	1.01	0.04	-2.42
753	-0.52	0.15	0.83	0.88	0.02	-2.36
761	-0.23	-0.05	0.68	0.75	0.22	-1.61
778	-0.49	0.16	0.92	0.88	0.02	-2.31
865	-0.70	0.14	0.85	0.87	-0.11	-2.12
885	-0.64	0.15	0.82	0.88	-0.08	-2.15
900	-0.92	-0.06	0.43	0.60	-0.30	-2.41

Table 4: LUTs of the mean-bias shift as small-large PICS as a function of the wavelength of MERIS.

9. Known limitations of the TOA simulations

9.1. Retrieval of BRDF model parameters in the MERIS spectral bands with significant water vapour and O2 absorption

The retrieval of BRDF model parameters over the PICS in the MERIS spectral bands with significant absorption from water vapour and O2 results into larger RMSE between the simulated and measured MERIS observations 709 nm, 761 nm and 900 nm than in neighbouring spectral bands not sensitive to absorption from these gas (red curves in Figure 3). There are two explanations for this larger residual RMSEs. First, the absorption cross sections used for the modelling of these gases might be inaccurate. Second, there is an additional variability in the TOA reflectance at 709 nm, 761 nm and 900 nm (black curves in Figure 3). Water vapour absorption is influenced by the natural spatio-temporal variability water vapour concentration. This might not be sufficiently well captured by the ERA-Interim water vapour fields. O2 absorption is mostly influenced by surface pressure

variations that are not accounted for in the TOA simulations. Moreover, other physical factors might influence the absorption in both bands such as the atmospheric temperature and aerosol optical properties and vertical distribution.

These bands were thus excluded from the bands used to retrieve the hyperspectral BRDF model parameters and the parameters values obtained at 709, 761 and 900 nm from MERIS observations (black stars in the Figure 2) are often seen to depart from the hyperspectral model (red line in the Figure 2)

9.2. Spectral interpolation of the surface BRDF model between the MERIS spectral bands

It is interesting to simulate the full archive of MERIS TOA observations over the PICS using the hyperspectral BRDF model parameters (derived from 4 years of MERIS data only) to measure the performance of the model, i.e., it's ability to reproduce the MERIS observations over the full archive (Figure 7 and Figure 8). One would expect that the MERIS simulated TOA reflectances obtained using the hyperspectral BRDF models retrieved over each PICS as input to the simulation should allow reproducing the MERIS TOA observations to within the RMSE in Figure 3 and with the accuracy indicated in Figure 4.

Figure 7 shows that this is not always the case in the absorption bands at 709 nm, 761 and 900 nm (for the reasons detailed in the previous section).

One can also observe that at 490 nm and 510 nm (Figure 7), the simulation of MERIS TOA observations for the Libya-1 site are not consistent with those obtained at other sites. This can be explained by the fact that the hyperspectral RPV model parameters derived for each site (red line in Figure 2) do not perfectly agree with the multi-spectral RPV model parameters (black stars in Figure 2 derived from MERIS TOA data inversion. This is for instance visible at 490 nm and 510 nm for Libya-1 where a slight difference can be observed for the ρ_0 parameter (Figure 2). This is not observed for this other PICS sites. This disagreement in the BRDF model parameter ρ_0 explain the fact that the Libya-1 results at 490 nm and 510 nm in Figure 7 appear as outliers.

The differences of the mean bias of the simulation over the small to large PICS show that the highest discrepancy can be observed over the short wavelengths <600 nm, and particularly the greenish bands around 450-560 nm, where the bands are more sensitive to the BRDF effects.

10. Uncertainties of the TOA simulations

10.1. Spectral bands with marginal water vapour and O2 absorption

We can distinguish the random and systematic uncertainty associated to the simulations of TOA reflectances.

10.1.1. Random uncertainties estimation

The random uncertainty associated to the TOA simulation of sensors with spectral bands without significant absorption from water vapour and O2 should be of the same order of the RMSE obtained in the spectral bands of MERIS, i.e, in the range of 1% to 4% (see Figure 3). This is

confirmed by the standard deviations associated to $\frac{\rho_{\mathrm{obs}}^{\mathrm{TOA}}(\lambda)}{\rho_{\mathrm{sim}}^{\mathrm{TOA}}(\lambda)}$ time series obtained on the full MERIS archive over all 6 PICS sites in Figure 8.

Figure 3 indicates that Libya-4 should provide the lowest random uncertainties while the Algerian sites should provide the highest.

The random uncertainty assigned to each acquisition simulation for any site and any wavelength is not affected by water vapour or O2 absorption, thus it is conservatively estimated to 4 % (k=1) or 8% (k=2).

The absolute differences in the standard deviation between the small to large PICS are less than 2% (Figure 9), which is lower that the random uncertainty per site (e.g. 4%). This illustrates that one can use the hyperspectral BRDF over the small PICS without significant impact on the random uncertainty.

10.1.2. Systematic uncertainties estimation

The systematic uncertainties associated to the TOA simulations over a given site have two origins:

1. The residual bias after the surface BRDF model parameters in MERIS bands were retrieved (Figure 4). This is below 1% and varies from site to site and band to band.
2. The mismatch between the hyperspectral BRDF parameters and the same parameters derived from the inversion of the MERIS reference data at the MERIS spectral band central wavelengths. This is mainly due to the fact that the derivation of the hyperspectral ρ_0 variations is based on a least square fit between the 12 MERIS spectral ρ_0 values and 8 linearly combined *eigen* spectral from the hyperspectral database of surface reflectances.

In both cases, the systematic uncertainty contributors should be site dependant and using several sites should reduce the systematic uncertainty from a single site. This seems to be the case in Figure 8: the mean ratio $\frac{\rho_{obs}^{TOA}(\lambda)}{\rho_{sim}^{TOA}(\lambda)}$ over all sites for the MERIS 3rd reprocessing archive is below 1 % for all bands not affected by water vapour and O2 absorption.

When using only individual sites, the systematic uncertainty can reach ~5 % as discussed for Libya-1 in section 9.2.

The absolute differences in the bias between the small to large PICS are less than 3% (Figure 9) except the greenish bands of Algeria3, which seems to be outliers. However, these differences are lower that the systematic uncertainty per site (e.g. ~5%), which leads to consider that the contribution of the hyperspectral BRDF over the small PICS is already included in the systematic uncertainty.

Note that, when using the 6 sites, the systematic uncertainty associated to each simulation is estimated to 1 %.

10.2. Spectral bands with significant water vapour and O2 absorption: 709 nm, 761 nm and 900 nm

10.2.1. Random uncertainties estimation

The random uncertainty associated to the TOA simulation of sensors with spectral bands with significant absorption from water vapour and O2 should be of the same order of the RMSE obtained in the spectral bands of MERIS, i.e, in the range of 2% to 6% (Figure 3).

The random uncertainty assigned to each acquisition simulation for any site is thus conservatively set to 6 % (k=1) or 12% (k=2).

10.2.2. Systematic uncertainties estimation

The systematic uncertainty associated to the TOA simulation of sensors with spectral bands with significant absorption from water vapour and O2 is more difficult to assess. It was previous discussed that it might have different origins (inaccuracy of the absorption cross-sections, non-modelled atmospheric temperature/pressure variability and vertical distribution). It was rather set to conservative values roughly commensurate with the level of absorption in these spectral bands: 5 %, 50 % and 50 % respectively for band 709, 761 and 900 nm.

11. Conclusion

Hyperspectral BRDF model parameters were derived for the 6 CEOS PICS from 4 years of MERIS 3rd reprocessing data.

These hyperspectral BRDF model parameters can be used in DIMITRI to simulate TOA reflectance for any sensor.

The uncertainty budget was broken down into system and random uncertainties for spectral regions with or without water vapour and O2 absorption.

Although the Hyperspectral BRDF model can be used over small-PICS, it is worth to derive a BRDF model associated to the small PICS to re-assess the correction LUTs in Table 4

References

- Bouvet M., Radiometric comparison of multispectral imagers over a pseudo-invariant calibration site using a reference radiometric model, *Remote Sensing of Environment 140 (2014) 141–154*

- Bullard, J.E., White, K., (2002). Quantifying iron oxide coatings on dune sands using spectrometric measurements: An example from the Simpson-Strzelecki Desert, Australia, Journal of Geophysical Research, Vol. 107, NO. B6, 2125

- Cosnefroy, H., Leroy, M. and Briottet, X. (1996). Selection of Sahara and Arabia desert sites for the calibration of optical satellite sensors. Remote Sensing of the Environment, 58, 101-114

- Hess, M., Koepke, P., & Schult, I. (1998). Optical properties of aerosols and clouds: The software package OPAC. Bulletin of the American Meteorological Society, 79, 831–844.

- Rahman, H., Pinty, B., & Verstraete, M. M. (1993). Coupled surface-atmosphere reflectance (CSAR) model, 2, Semi empirical surface model usable with NOAA ad- vanced very high resolution radiometer data. Journal of Geophysical Research, 98(D11), 20,781–20,801.